Monosaccharides *versus* PEG-Functionalized NPs: Influence in the Cellular Uptake

María Moros,[†] Bruno Hernáez,[‡] Elina Garet,[§] Jorge T. Dias,[†] Berta Sáez,[†,⊥] Valeria Grazú,[†,*] África González-Fernández,[¶] Covadonga Alonso,[‡] and Jesús M. de la Fuente[†,*]

[†]Biofunctionalization of Nanoparticles and Surfaces (BioNanoSurf), Instituto de Nanociencia de Aragón, Universidad de Zaragoza, Mariano Esquillor, s/n, 50018, Zaragoza, Spain, [‡]Departamento de Biotecnología, Instituto Nacional de Investigación y Tecnología Agraria y Alimentaria, INIA, Autovía A6 km 7,5, 28040, Madrid, Spain, [§]NanoImmunoTech SL, Pza. Fernando Conde, Montero Ríos 9, 36201, Vigo, Spain, [⊥]Instituto Aragonés de Ciencias de la Salud, Avda. Gomez Laguna 25, 50009, Zaragoza, Spain, and [¶]Inmunology, Biomedical Research Center (CINBIO), University of Vigo, Campus Lagoas Marcosende s/n, 36310, Vigo, Pontevedra, Spain

ABSTRACT Magnetic nanoparticles (NPs) hold great promise for biomedical applications. The core composition and small size of these particles produce superparamagnetic behavior, thus facilitating their use in magnetic resonance imaging and magnetically induced therapeutic hyperthermia. However, the development and control of safe *in vivo* applications for NPs call for the study of cell—NP interactions and cell viability. Furthermore, as for most biotechnological applications, it is desirable to prevent unspecific cell internalization of these particles. It is also crucial to understand how the surface composition of the NPs affects their internalization capacity. Here, through accurate control over unspecific protein adsorption, size distribution, grafting density, and an extensive physicochemical characterization, we correlated the cytotoxicity and cellular uptake mechanism of 6 nm magnetic NPs coated with several types and various densities of biomolecules, such as glucose, galactose, and poly(ethylene glycol). We found that the density of the grafted molecule was crucial to prevent unspecific uptake of NPs by Vero cells. Surprisingly, the glucose-coated NPs described here showed cellular uptake as a result of lipid raft instead of clathrin-mediated cellular internalization. Moreover, these glucose-functionalized NPs could be one of the first examples of NPs being endocytosed by caveolae that finally end up in the lysosomes. These results reinforce the use of simple carbohydrates as an alternative to PEG molecules for NPs functionalization when cellular uptake is required.

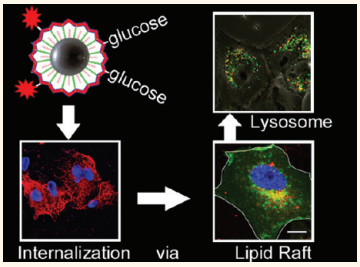

KEYWORDS: biofunctionalization · carbohydrates · cellular uptake · cytotoxicity · magnetic nanoparticles

The great interest in nanotechnology has led to an increase in the number of new nanomaterials that can potentially be used in biomedical applications.[1] Among the nonbiodegradable materials, metallic nanoparticles (NPs) are one of the most prominent and have been used for several applications in the field of biotechnology for the last 20 years.[2]

These NPs are generally composed of an inorganic core, and an organic shell that stabilizes these structures in a biological suspension. The inorganic core consists of noble metals, magnetic materials, semiconductor nanocrystals and others, which, because of their size, have physical properties of interest for the development of novel sensing and diagnosis tools, as well as innovative therapy strategies.[3,4]

The first designs of biotechnological applications using NPs were tentative; however, research performed in recent years has shown the relevance of the correct composition and structure of both the inorganic and organic components of the NP.[5] The physical properties of these particles are now tunable as they are influenced by the composition, shape, size, and crystallinity of the inorganic core. The organic shell, located in the most external part of the NP, provides the chemical functionality to the nanostructure, and it is responsible for the solubility, stability, charge effect, and interactions with other molecules.[6] Not only are the inorganic core composition, size and organic shell crucial parameters for biomedical applications, but so is biofunctionalization with targeting molecules, such as peptides or antibodies, as this procedure is frequently required to provide a biological functionality, thus leading to active targeting of tissues or cells.[7]

Moreover, in order to use these new materials in biomedical applications, it is of the upmost importance to achieve their stability in physiological conditions as well as to minimize unspecific interactions with other biomolecules present in the media.[8] Up until now, poly(ethylene glycol) (PEG) has been used for this purpose.[9] A dense

* Address correspondence to vgrazu@unizar.es, jmfuente@unizar.es.

Received for review November 22, 2011 and accepted January 3, 2012.

Published online January 03, 2012
10.1021/nn204543c

layer of PEG confers hydrophilicity to nanomaterials, thereby increasing their solubility in water, but this polymer also prevents unspecific interactions with other molecules. Recently, our research group demonstrated the efficiency of monosaccharides such as glucose for this purpose.[10] These small saccharidic molecules have several advantages: they do not increase the global hydrodynamic size of the NP, they are easy to work with, and they are inexpensive. Furthermore, their small size does not give rise to the shielding of other conjugated ligands, in contrast to what occurs when using PEG chains.[11]

Monosaccharides could be used as passivation molecules but may also serve as targeting molecules, as carbohydrates present in the organism play a major role in many biological processes. In fact, carbohydrates are involved in a variety of biological functions, such as cell–cell signaling, adhesion, cell migration, and cancer development and metastasis.[12,13] However, few studies have addressed the complex nature of the interactions of sugar-modified NPs with cells, where the carbohydrate attached determines the degree and route of NP internalization.[14] It has been shown that NPs functionalized with carbohydrates allow the detection and profiling of various cell types on the basis of the carbohydrate–receptor interaction;[15] the uptake of NPs functionalized with lactose or glucose was reported to be faster than that of unmodified NPs in cancer cells,[16] and also, galactose NPs have been used effectively *in vivo* for liver targeting.[17,18] In all these examples, NPs functionalized with carbohydrates interact with molecules located in the cell membrane.

Furthermore, carbohydrate-functionalized NPs could have another potential role, namely, overcoming biological barriers such as the plasma membrane or the blood–brain barrier.[19] The systematic study of how NPs overcome the plasma membrane is crucial since the targeted subcellular compartments differ depending on the route selected. Generally, endocytic pathways can be divided in two broad categories, phagocytosis and pinocytosis. The former is a critical step that occurs mainly in specialized cells, and it is intended to defend the organism against exogenous elements.[20] Nonphagocytic pathways can occur virtually in all cells and can be divided into clathrin- and nonclathrin-dependent endocytosis. The latter can then be split into three main mechanisms: macropinocytosis, caveolae-mediated endocytosis, and clathrin- and caveolae-independent endocytosis.[21] The rate and mechanism of NP uptake is cell type-dependent and varies with NP size, charge, and other surface properties.[22,23] It has been reported for instance that, once internalized into the cell, saccharide-coated NPs are trapped in endocytic vesicles.[24] Also, NPs coated with cationic glycopolymers are released to the cytoplasm as a result of endocytic vesicle disruption mediated by the cationic moiety.[25]

Therefore, the functionalization of a NP with a single carbohydrate moiety could confer this structure three capacities (blocking protein unspecific adsorption, active cell targeting, and cell internalization) when multifunctionalization is usually required to achieve this goal. Given the huge potential of NPs and in order to further characterize these challenging materials, it is important to study their cellular uptake as well as their potential toxicity. Here we performed systematic studies to evaluate the cellular internalization route of carbohydrate-functionalized magnetic NPs with a diameter of 6 nm, as well as an extensive set of cytotoxic assays. To the best of our knowledge, this is the first study to address the endocytic routes of carbohydrate-functionalized NPs and internalization fate during distinct periods of time, combined with a range of cytotoxic studies.

Moreover, we describe that the cellular uptake of NPs is largely dependent on the type and density of carbohydrate attached to their surfaces. Our studies demonstrate that carbohydrate-modified metal NPs are nontoxic and represent an advance in the field, in which few examples can be found.[26]

RESULTS AND DISCUSSION

NP Functionalization. Monodisperse iron oxide NPs with an average diameter of 6 nm were synthesized following a seed-mediated growth procedure previously described.[27] These NPs are prepared in organic solvents and coated with oleic acid, thus requiring further treatment for transfer to an aqueous solution. We therefore followed a modified version of a previously reported methodology,[28] using an amphiphilic polymer shell, poly(maleic anhydride-alt-1-octadecene) (PMAO) to transfer the NPs to water.[10] The hydrophobic part of the polymer consists of 18-carbon alkaline side residues that intercalate and interact hydrophobically with the oleic acid chains that cover the NPs. The hydrophilic part of the polymer, the maleic anhydride moieties, is exposed to the outermost part of the NP, thus conferring stability. It also provides useful reactive groups for further functionalization. The hydrolysis of the external maleic anhydride groups of the polymer shell in water renders two carboxylic groups per monomeric unit of maleic anhydride. Treatment of NPs in basic conditions with NaOH 0.05 M, followed by the complete evaporation of the chloroform, provides carboxylated NPs that are fully soluble in water. Opening of the anhydride groups can also be achieved using nucleophiles such as alcohols, primary or secondary amines, and thiols, so the polymer can be modified before transferring the NPs to aqueous solutions. The excess of unbound polymer is then removed *via* centrifugation.

Multifunctional NPs were prepared by incorporation of a fluorescent dye (tetramethylrhodamine 5-(and -6)-carboxamide cadaverine, TAMRA) and either glucose

(Glu), galactose (Gal), or poly(ethylene glycol) (PEG), to passivate the NP surface. Two functionalization strategies were followed (Scheme 1). The first involved a competitive protocol (group A NPs), where the dye and the passivation molecules (monosaccharides or PEG) were incorporated simultaneously. Amine-modified derivatives of the monosaccharides (Glu or Gal) or PEG and TAMRA were added to the NPs previously activated with *N*-(3-dimethylaminopropyl)-*N*′-ethylcarbodiimide hydrochloride (EDC) (Scheme 1A). The second functionalization strategy consisted of a stepwise (sequential) process (group B NPs). NPs were coated with chemically modified PMAO where TAMRA was previously incorporated to 1% of the total PMAO monomers. After that, the passivation was followed as described earlier (Scheme 1B).

NPs functionalized by the competitive strategy had a greater number of dye molecules attached than when prepared by the sequential strategy (see Supporting Information, Figure S1 and S2). Control over the competitive strategy is difficult to achieve as the number of molecules incorporated depends on various parameters such as the size and reactivity of the amine-derived fluorescent dye or passivation agents. As a result of the higher amount of dye molecules per NP obtained using this strategy, there is a decrease in the number of passivation molecules per particle.

We evaluated the efficiency of the passivation by zeta (Z)-potential measurements, a common technique when determining the presence of distinct coatings (Figure 1).[29] Clear differences between the NPs obtained with the two strategies were found.

Passivation molecules are neutral and TAMRA is a positive molecule. Thus, the less negative Z-potential of the TAMRA **NP A** compared to the TAMRA **NP B** shows that this strategy allows the incorporation of a higher amount of fluorophore. Having the TAMRA NPs as a reference, the incorporation of the passivation molecules was confirmed by the decrease of the Z-potential, as a result of the surface charge neutralization. The larger difference in the Z-potential values between TAMRA NPs and the passivated NPs in Group B also indicate a higher density of passivation molecules on the particle surface when this stepwise strategy was followed. It should be highlighted that the Z-potential for PEG **NP B** was near zero as a result of the flexibility of the PEG chains and an almost complete covering of the NP surface. Moreover, gel electrophoresis showed a narrow band in almost every case, implying a narrow NP distribution and similar sizes for Glu and Gal NPs,[30] also evaluated by dynamic light scattering and transmission electron microscopy (Supporting Information, Figures S3, S4, and S5).

Cytotoxic Assays. While bare iron oxide NPs are slightly cytotoxic, coated superparamagnetic iron oxide nanoparticles (SPIONs) are traditionally considered relatively nontoxic.[31] However, in terms of cytotoxicity, many

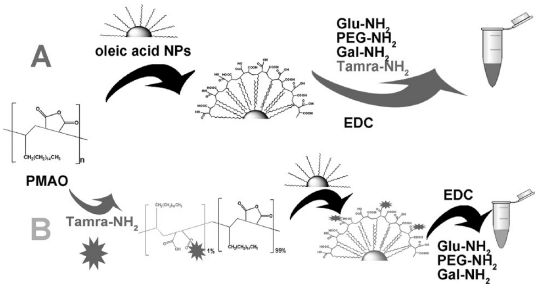

Scheme 1. Strategies used to multifunctionalize the NPs with a passivation agent and a fluorescent dye. NPs synthesized in a competitive way (A) imply water transfer of oleic acid-capped NPs, prior to the incorporation of the dye and the passivation agents (glucose, galactose, and PEG) onto their surface. The second functionalization strategy (B) requires the chemical modification of the polymer with the dye before using it to transfer the oleic acid-capped NPs into water. After the hydrolysis of the remaining anhydride groups, the next step involves functionalization with only passivation reagents

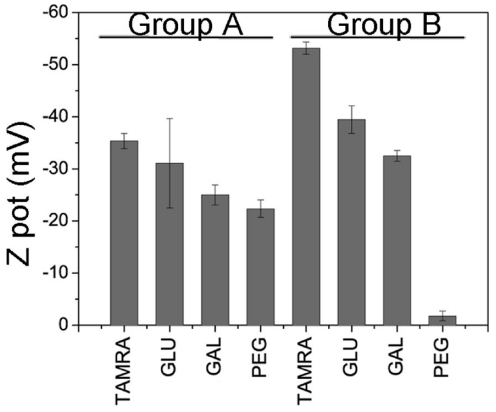

Figure 1. Zeta potential measurements performed for both sets of NPs at pH 7.4, presented as the mean of 10 runs ± SD.

factors such as the test performed, the NP composition, and concentration, the cell line or the time schedule have to be taken into account when conducting the assays. The combination of various experiments and cell lines is crucial for assessing toxicity.

To assess the NP toxicity on cells, we performed several sets of experiments (viability assay, ROS production, and cell cycle disruption) by incubating distinct cell lines with NPs. Moreover, the potential inflammatory reaction induced by these structures was also tested by *in vitro* analysis, checking the activation of the complement cascade by Western blot analysis of C3 factor degradation.

Although there are no standardized protocols for assessing cytotoxicity, it has been suggested that given the differences in the cell line origin, proliferation state or membrane characteristics, among others, distinct types of cells should be used to test NP cytotoxicity.[32] Thus, we performed cell viability studies with 50 and 100 μg mL^{-1} of each NP group on four cell lines [HeLa (human cervical cancer cells), A549 (lung

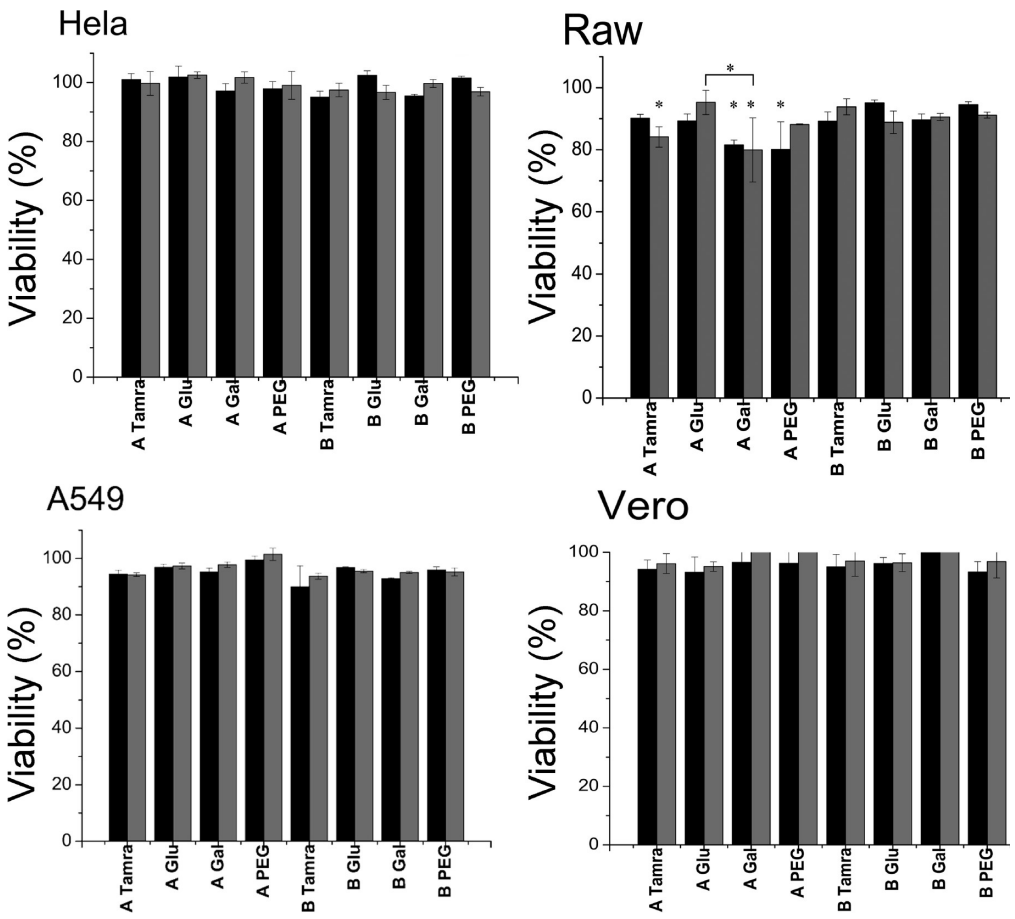

Figure 2. Viability assay performed with various cell lines. Black bars correspond to experiments where the NP final concentration was 100 μg mL^{-1}, whereas gray bars correspond to those in which the final concentration of NPs was 50 μg mL^{-1}. A stands for Group A NPs and B stands for Group B NPs. A *P* value less than 0.01 was considered statistically significant.

carcinoma cells), Vero (monkey kidney epithelial cells), and Raw 264.7 (mouse leukemic monocyte/macrophage cell line)], and during 48 h of incubation (Table 1, Supporting Information). To perform these assays, the number of cells was first optimized to avoid interferences with cell viability occurring because of limited nutrients. Cell viability was measured using the Quick Cell reagent, which is reduced by the dehydrogenases in living cells (Figure 2).

Cell viability was largely dependent on the cell line, Raw 264.7 cells being the most sensitive to NPs. Nevertheless, cell viability was greater than 80% in all the cases, and little difference was found between naked, PEG-, Glu- or Gal-coated fluorescent NPs except in Raw cells. As mentioned before, few studies have addressed the toxicity of carbohydrate-modified NPs using several cell lines. In this regard, it has been reported that silver NPs modified with glucose or lactose have a slight toxic effect at 30 μg mL^{-1} after the second day of incubation when using A549 cells.[16] In other studies, maltose-modified gold NPs proved highly cytotoxic while glucose-modified ones showed no effect.[14] These observations indicate that both the NP and the carbohydrate participate in the toxic effect.

Another main issue when studying cytotoxicity is the production of ROS, as cell toxicity can be produced directly, but also indirectly, by an excess of ROS generation,[33] which can damage various molecular targets, including DNA, protein, and lipids. We analyzed ROS by flow cytometry using HMy (human lymphoblastoid B leukemia) cells. This tumoral cell line was chosen because of its high sensitivity to low amounts of ROS generation when it is treated with other NPs.[32] None of the NPs tested showed ROS production in the conditions assayed (Supporting Information, Figure S6). Previously, it was demonstrated that 4 nm iron oxide NPs coated with citrate induce the generation of ROS, which can result in severe cell dysfunction, even when the cells do not show cytotoxicity using conventional cellular viability assays.[34] However, the induction of ROS using iron oxide NPs remains complex. Gao and co-workers reported that bare magnetic iron oxide NPs exhibit peroxidase-like activity, which can reduce the amount of hydrogen peroxide present in the cell, thus stimulating cell proliferation.[35]

We also analyzed the effect of NPs on cell cycle, as DNA damage can be evidenced in cell cycle progression.

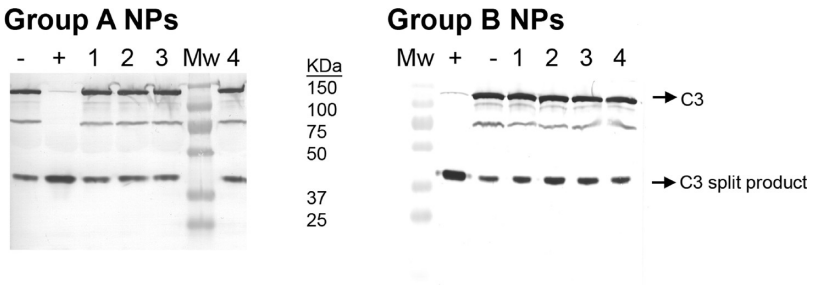

Figure 3. Analysis of complement system activation by Western blot of both groups of NPs: (−) negative control (PBS); (+) positive control (cobra venom factor); (1) TAMRA-labeled NPs; (2) glucose (Glu) NPs; (3) galactose (Gal) NPs; (4) PEG NPs. MW corresponds to the molecular weight of the protein marker (kDa).

The cell cycle is a vital process responsible for cell division and duplication. In eukaryotes this cycle can be divided into two phases: the interphase, in which the cell grows and accumulates nutrients, and the mitosis (M) phase, in which the cell splits into two. The interphase comprises three parts: G1, S, and G2. Deregulation of the cell cycle phases may lead to tumor formation.[36] Each phase of the cell cycle exposed to the NPs was analyzed by flow cytometry, assessing any deregulation of the cycle that results in the accumulation of cells in one or more phases. We found that at a NP concentration of 100 μg mL^{-1} no cell arrest occurred in any of the phases (Supporting Information, Figure S7). Mahmoudi *et al.* reported that the cell cycle is affected only by very high concentrations of 48 and 85 nm bare and poly(vinyl alcohol)-coated iron oxide nanobeads.[37] In contrast, 6−20 nm starch-coated silver NPs showed a G2/M arrest at 25 μg mL^{-1}.[38]

Finally, the potential inflammatory reaction induced by NPs was studied by assessing the activation of the complement system. This system comprises a very complex group of proteins that can be activated through several pathways (classical, alternative, or lectin-mediated). Although its main function is the opsonization and clearance of invading agents, the complement system also mediates inflammation, favors phagocytosis, and targets cell death.[39] A critical step in the activation of this system consists of the cleavage of the complement component 3 protein (C3). Although this protein shows spontaneous and basal degradation, its cleavage is considerably increased after activation of the complement cascade by any of the three pathways. To examine whether NPs have potential effects on the complement activation cascade, we analyzed C3 degradation by electrophoresis followed by Western blot analysis with antibodies directed against C3. None of the NPs assayed promoted C3 cleavage (Figure 3). While the band corresponding to C3 almost disappeared in the positive control (increasing in accordance with the intensity of the C3 split product), no major differences were found in plasma incubated with NPs compared to the negative control (plasma incubated with PBS). Similar results have been described for 30 and 50 nm citrate-capped gold NPs,[40] whereas carbon nanotubes and different-sized core shell polysaccharide NPs cause complement activation.[41,42]

Cellular Uptake of Functionalized NPs. To clarify and demonstrate the relevance of the functionalization strategies on the NP−cell interaction, we performed cell uptake experiments using the Vero cell line, all of which were done under the same conditions for all NPs.

First, the internalization mechanism of NPs was studied by incubating cells with all the NPs at 4 and 37 °C. NPs kept at 4 °C were not internalized and remained attached on the surface membrane (Supporting Information, Figure S8), while at 37 °C some NPs were internalized into the cytoplasm. Therefore, the cellular uptake of these NPs is most likely energy-dependent.[43]

The internalization of the NPs obtained through the competitive and sequential strategies was assessed to compare and infer about the influence of the functionalization protocol. All NPs functionalized with the competitive strategy (group A NPs) were internalized in higher amounts after 15 min of incubation at 37 °C (Figure S9), compared to the NPs functionalized with the sequential strategy (group B NPs) (Figure 4). Furthermore, clear differences between PEG, Glu, and Gal NPs were detected in group B NPs, due only to the nature of each functionalized biomolecule, as aggregation induced by culture media conditions did not occur (Supporting Information, Table S2 and Figure S9). The rate and the intracellular fate of NP uptake by cells depends on many factors, such as charge, size, hydrophobicity, or even the ligand arrangement.[44−47] Moreover, the uptake mechanism may be different depending on the cell line.[48] To date, PEG is one of the most widely used inertization agents as it provides steric stabilization and prevents serum protein absorption, which is the greatest limit for long-time circulating half-life.[49] Proteins adsorbed on the NP surface promote opsonization, leading to aggregation and/or clearance from the bloodstream.[50] Therefore for *in vivo* applications of NPs it is essential that the grafted PEG covers the NP surface sufficiently in order to efficiently prevent opsonization and to hinder the

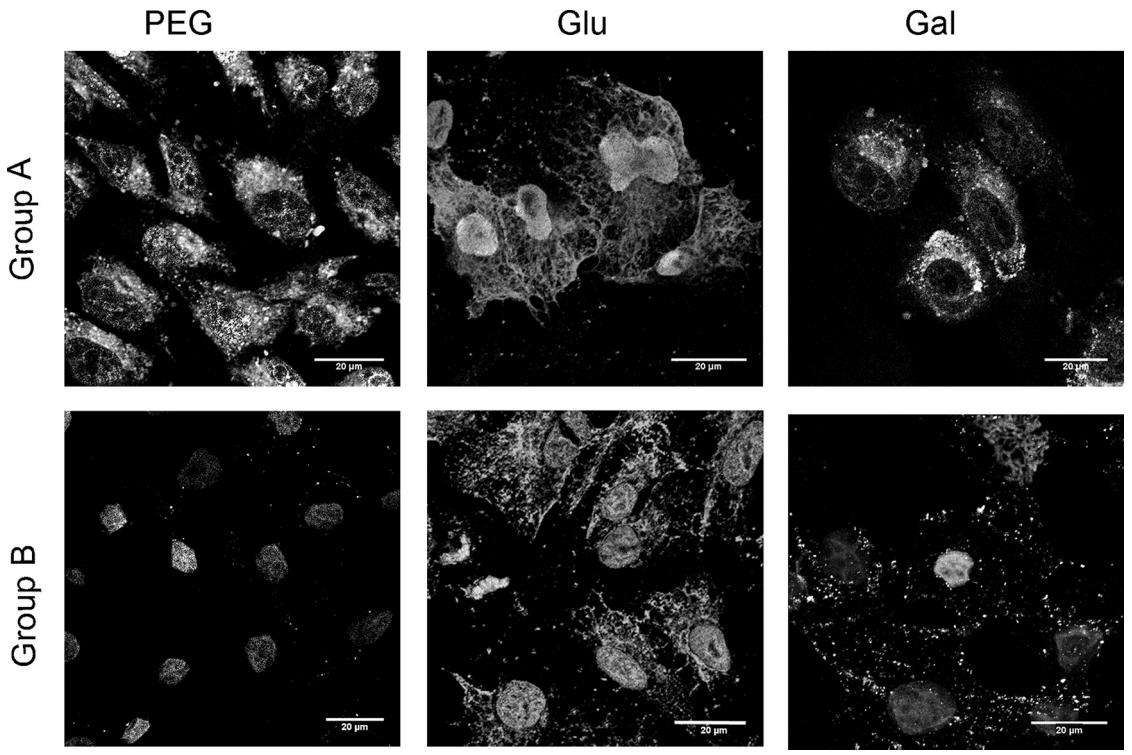

Figure 4. Confocal micrographs taken after 15 min of incubation of TAMRA-labeled NPs at 37 °C in Vero cells. PEG, glucose (Glu), and galactose (Gal) NPs produced in a competitive method (group A) entered the cell in all cases. While the uptake of PEG NPs produced in a sequential method (group B) was fully inhibited as a result of the PEG surface graft, Glu NPs in this group were internalized in only 15 min, while Gal NPs remained in the periphery. Scale bar = 20 μm.

unspecific uptake of the NPs by cells.[51] In this study, the uptake of NPs grafted with a high density of PEG was prevented, whereas NPs that exhibited less PEG, and therefore remained negatively charged, entered the cell in a massive way.

Although Glu and Gal NPs were internalized (group B), the cellular distribution for each differed. While Glu NPs entered throughout the cell, Gal NPs remained predominantly on the cell periphery, or attached to the membrane. Interestingly, these two types of NP share the same inorganic core, hydrodynamic size and Z-potential values, differing only in the type of carbohydrate. Hence, the difference in the cell entrance pattern can be attributed exclusively to the monosaccharide functionalized on the NP surface, that is to say Glu or Gal. Interestingly, glucose and galactose share the same chemical formula, except for the conformation of the hydroxyl group placed in C-4.

The internalization rate of Glu NPs (group B) was followed during the first 24 h. During the first 15 min, these particles were observed throughout the cytoplasm. As time increased, from 4 to 24 h, the NPs were observed in large clusters. This finding may indicate that they were being processed by other compartments (Supporting Information, Figure S10). Gal NPs had slower internalization kinetics than Glu NPs, although after 4 h of incubation they were detected inside the cell (data not shown). NPs modified with TAMRA, without further functionalization, did not enter the cells. This finding could be explained by aggregation problems in the cell culture media, as large aggregates were observed surrounding the cells (Supporting Information, Figure S11). This observation reinforces the idea that correct functionalization is compulsory when studying NP uptake. Moreover, not only is the type of coating crucial for cell uptake but so is the density of components on the surface.

Mechanisms of NP Cellular Uptake. To study the endocytic mechanisms involved in NP uptake, we used Glu NPs functionalized by the sequential strategy.

First of all, we used SEM microscopy to study morphological cellular changes in cells incubated with Glu NPs. Differences in membrane structures were not observed when compared with control cells (Supporting Information, Figure S12). The influence of these NPs *in vitro* was also assessed in terms of fluorescent observation of cytoskeleton (actin, tubulin, and vinculin), finding no differences with control cells (Supporting Information, Figure S13).

For many years, clathrin-mediated endocytosis has been the most studied cellular entry pathway; clathrin-independent pathways include caveolar endocytosis, macropinocytosis, and clathrin- and caveolae-independent pathways; the latter are subclassified as Arf6-dependent, flotillin-dependent, Cdc42-dependent, and RhoA-dependent,[52] although ongoing research may lead to the characterization of other routes. Colocalization studies of Glu NPs and caveolae or clathrin were

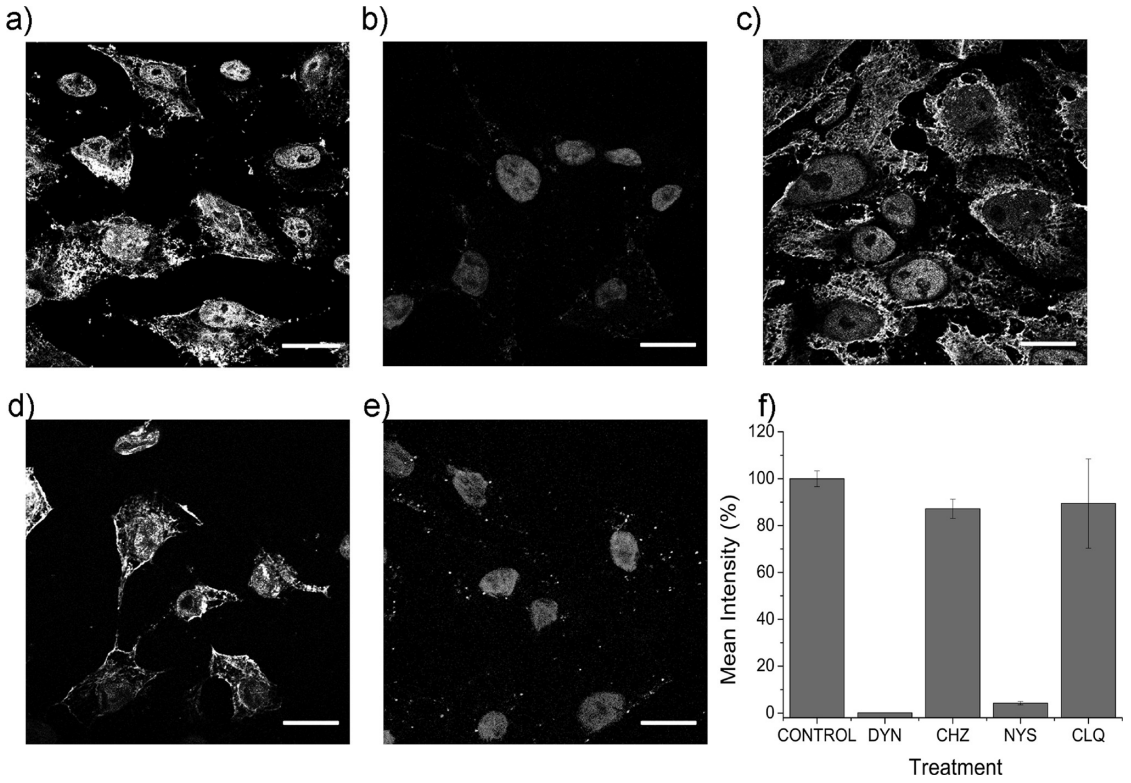

Figure 5. Study of glucose (Glu) NP uptake by means of inhibitors. (a) Glu NP uptake without further treatment and cells treated with (b) dynasore (DYN) 80 μM, (c) chlorpromazine (CHZ) 14 μM, (d) chloroquine (CLQ) 20 μM, and (e) nystatin (NYS) 50 μM. (f) Graph representing the mean intensity of TAMRA fluorescence in each sample after analyzing the cells using confocal microscope software. Scale bar = 20 μm.

carried out by incubating cells with NPs, fixating and staining using fluorescent anticaveolin 1 and anti-clathrin antibodies. Colocalization was not observed (Supporting Information, Figure S14). However, the NPs amount and/or pattern in the permeabilized and stained cells differed from those used without permeabilization solution (Supporting Information, Figure S15). These differences indicate that the fixation and permeabilization procedure affect NP localization. In fact, it has been reported that the distribution of certain lipid compartments are sensitive to fixation conditions.[53−55] Therefore, the change in NP distribution pattern may be attributable to a poor fixation of the compartments in which they were retained and consequently loss of the content. To prevent this from happening, the internalization mechanisms were studied by means of drug inhibitors.

Clathrin- and caveolae-mediated pathways, as well as others lipid raft routes, require dynamin.[56,57] This molecule is a 100 kDa GTPase that has an essential role during the vesicle formation of coated pits and caveola derived vesicles.[58] To inhibit the GTPase activity of dynamin, we used dynasore (DYN).[59] Treatment with DYN prevented the internalization of Glu NPs, thus indicating that NP uptake is a dynamin-dependent process (Figure 5b). The most studied dynamin-dependent routes are the clathrin and caveolar ones. Therefore, to assess which one is used for NP uptake, the inhibitory effect of chlorpromazine (CHZ) was tested. CHZ is a cationic amphiphilic drug that perturbs clathrin-processing and hence endocytosis by clathrin-dependent mechanisms.[60] CHZ was used at a concentration known to prevent Transferrin (TF) uptake in Vero cells without promoting cell detachment.[61] In this case, NP uptake was reduced by only 18% (Figure 5c), thereby suggesting that clathrin-mediated endocytosis is not the main route of internalization.

We next used the drug inhibitor chloroquine (CLQ). Lysosomotropic agents, such as CLQ, are nonspecific weak bases that diffuse across membranes in a concentration-dependent manner, thereby neutralizing the pH of endocytic vesicles.[62] Endosomal acidification is one of the hallmarks of clathrin-mediated endocytosis. Inhibition of this route using CLQ occurred at the endosomal level. Treatment with CLQ slightly affected the number of NPs internalized and their distribution inside the cell differed from that observed for the controls. Most NPs appeared to be retained on the membrane surface, indicating that the clathrin pathway (or other endosome-dependent route) may be used as a secondary or minor route for NP entry (Figure 5d).

In addition, we also analyzed the participation of caveolae/lipid rafts during Glu NP uptake. For this purpose, we used a drug that interferes with these internalization pathways, namely nystatin (NYS), a cholesterol-sequestering agent that disrupts the

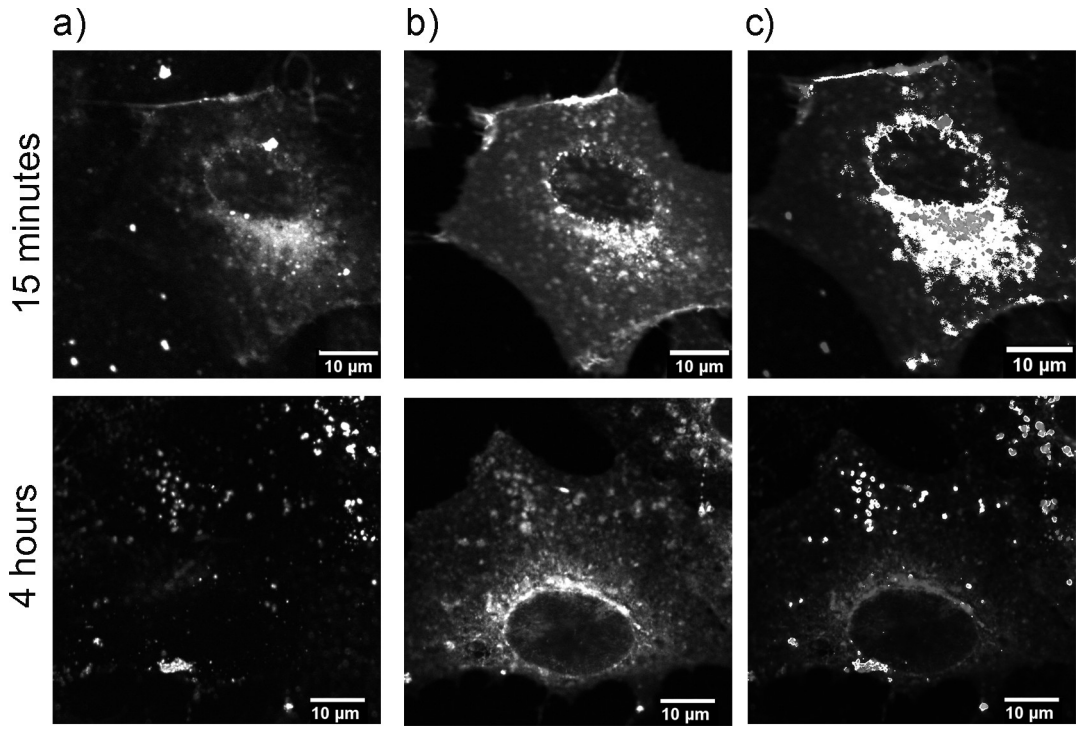

Figure 6. Cholera toxin colocalization with glucose TAMRA-labeled NPs was performed as this toxin is generally accepted as a lipid raft marker. Confocal microscope images from (a) glucose (Glu) NPs, (b) cholera toxin-labeled with Alexa-488, and (c) colocalizated pixels shown in white reveals the high grade of colocalization in 15 min of incubation. At 4 h this colocalization was found in smaller spots rather than diffused throughout the cell. Scale bar = 10 μm.

membrane lipid raft and consequently prevents caveola formation.[63] Pretreatment of Vero cells with this drug at a concentration known to inhibit cholera toxin uptake (data not shown) inhibited the uptake of the Glu NPs (Figure 5e). This observation shows that caveolae/lipid rafts are preferentially involved in the internalization of these NPs.

To ensure that the drug treatments that affected clathrin-mediated pathways were effective, all the experiments were carried out under the same conditions using Alexa594-labeled transferrin as a positive control (Supporting Information, Figure S16).[64]

To reinforce the idea that the caveola/lipid raft is the main route for NP endocytosis, we studied cell uptake using cholera toxin as a lipid raft marker.[65] Cholera toxin has been traditionally proposed as a caveolae marker, although depending on cell type, its entry mechanism may be not exclusive.[66] Cholera toxin and Glu NPs showed high colocalization inside the cell (Figure 6).

Glu NP uptake was inhibited using a cholesterol-depletion agent, NYS, which can affect multiple lipid-raft-dependent endocytic pathways, including caveolar endocytosis. The complete inhibition of uptake achieved with DYN is consistent with caveolar pathway-mediated uptake while its role in other lipid raft-dependent routes has not yet been elucidated.[21] These results and the high degree of colocalization observed with the cholera toxin suggest that the caveolar route is the main mechanism involved in Glu NP uptake.

Although clathrin-mediated endocytosis has been traditionally proposed as the main route for NPs smaller than 200 nm,[67,22] caveolae can accommodate NPs up to 100 nm in diameter.[68] This observation is consistent with our data. Other lipid raft-dependent mechanisms may also participate in NP internalization, as they can lead to a more rapid ligand uptake than caveolae do, sharing the same mechanism proposed for negatively charged quantum dots.[69,70] It has been reported that the entry of cationic liposomes into the cell depends on the amount of ganglioside (GM1)-enriched lipid rafts, thus leading to a reduced uptake when many of these rafts are present.[71] Therefore, lipid rafts could have a preference for negatively charged NPs, like those proposed in the present study.

As previously reported,[72] Glu NP uptake is rapid. In that study the authors demonstrated that quantum dots capped with glucose interact with high-affinity glucose transporters in yeast cells, leading to a high uptake in only 10 min. Although performed in yeast, this result indicates that Glu NPs can be transported inside cells using a membrane carrier protein. Among the many glucose transporters, GLUT4 internalization has been described to be dynamin-dependent.[73] Therefore further studies are required to assess the potential of this transporter in Glu NP uptake.

To further study the localization of NPs after their internalization, we studied their colocalization with a

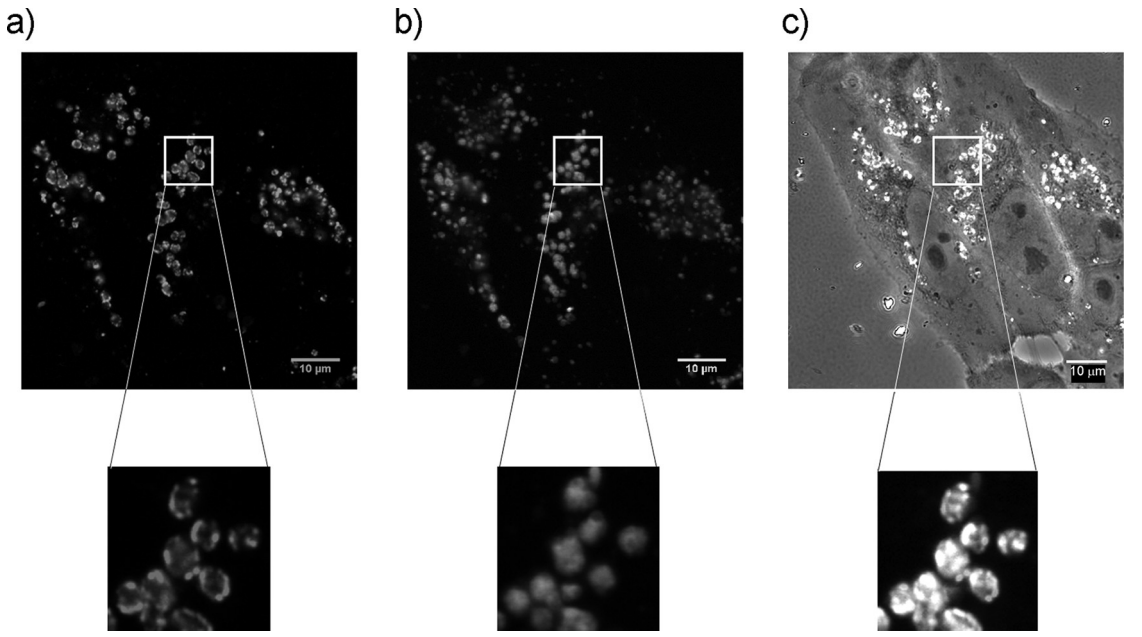

Figure 7. LysoTracker, a marker for acidic compartments was used to evaluate the localization of glucose (Glu) NPs in lysosomes after 12 h of incubation with cells. Live-cell imaging was performed with a confocal microscope. (a) Glu TAMRA-labeled NPs, (b) LysoTracker green, and (c) colocalized pixels in white superimposed over the bright field image. Scale bar = 10 μm.

subcellular structure, the lysosome. There are several examples of NPs terminated by lysosomes,[74−76] but in principle, NPs endocytosed by caveolae would avoid degradation in lysosomes.[77] Pelkmans and co-workers coined the term "caveosome" to name the endocytic compartment where the uncoated virus SV40 and caveolin were internalized after caveolae mediated uptake.[78] This compartment was not labeled by commonly used fluid phase markers and it was proposed to have neutral pH. Furthermore, it was proposed that cargos using the caveolar pathway would be spared from degradation in lysosomes, as they did not accumulate a lysosomal dye; therefore if Glu NPs enter the cell *via* this pathway, they should not show high colocalization with lysosomes. To study NP targeting to this organelle we loaded the cells with LysoTracker, a marker for acidic compartments and lysosomes, and performed live-imaging by confocal microscopy. Surprisingly, the degree of colocalization was high after 12 h of incubation (Figure 7), although this observation is commensurate with recent reports that propose that caveosomes are late endosomes/lysosomes from the normal endocytic pathway.[55] Using elegant approaches, they have demonstrated that, depending on its expression, caveolin 1 is targeted to lysosomes for degradation, thus the term caveosome should no longer be used. Therefore, studies describing the entry of NPs through caveolar-mediated endocytosis that assume that NPs would not be degraded in lysosomes should be reviewed. The Glu NPs described in this work could represent one of the first examples of NPs being endocytosed by caveolae that end up in the lysosomes.

CONCLUSIONS

Here we have shown that functionalizing the NP surface with carbohydrates, as well as the passivation of the particles, influences the cell uptake of these molecules. The type of monosaccharide used in the coating affects the rate of NP internalization into the cell. Therefore, simple carbohydrates represent an alternative to PEG molecules to graft onto the NP surface when cellular uptake is required. We also demonstrate that Glu NPs mainly follow a caveolar/lipid raft uptake, which culminates in lysosomes after 12 h of incubation. These cellular uptake studies were carried out with serum-free media to avoid interferences in the uptake mechanism caused by unspecific binding of serum proteins to NPs. Although previous studies performed with Glu NPs demonstrated that the absorption of model proteins such as bovine serum albumin was prevented,[10] carbohydrates could also interact with other serum molecules that form the *protein corona*, thus affecting the charge, coating, properties, and biodistribution of NPs. To address the *in vivo* application of these NPs, it would be pertinent to perform further studies addressing the effect of Glu NPs on the formation of the *protein corona* in human plasma.

To our knowledge, this is the first study to report in detail Glu NP cytotoxicity and cell uptake. As the uptake mechanism could depend on the cellular line, further studies must consider the use of different cell lines.

Given the involvement of carbohydrates in many pathological and nonpathological processes,[79] Glu NPs represent an interesting alternative for the development

of new theragnostic agents, gaining control over vectorization and cell internalization. Therefore, as reported here, systematic studies that address the cellular uptake of Glu NPs as well as their potential toxicity are needed before these challenging materials can be applied to *in vivo* applications.

METHODS

Unless otherwise stated, all the reagents were purchased from Sigma Aldrich.

Synthesis of water-soluble NPs. Monodisperse Fe_3O_4 NPs of 6 nm mean diameter were synthesized following the seed-mediated growth method described by Sun *et al.*[27] First, 4 nm Fe_3O_4 NP seeds were synthesized by mixing and stirring under a flow of argon, Fe(acac)3 (0.71 g), 1,2-hexadecanediol (2.58 g), oleic acid (2 mL), oleylamine (2 mL), solubilized in phenyl ether (20 mL) . The mixture was heated to 200 °C for 2 h and afterward heated to reflux (265 °C) under argon atmosphere for 1 h. The mixture was allowed to cool to room temperature by removing the heat source. The NPs were then washed with ethanol and collected with a magnet and redispersed in hexane. The process was repeated using these NPs as seeds to obtain 6 nm NPs. The transfer into water was performed using an amphiphilic polymer. A 250 mg aliquot of poly(maleic anhydride-alt-1-octadecene) (PMAO) was added to a flask containing 200 mL of chloroform. After the polymer was dissolved under magnetic stirring, 20 mg of the nanoparticles were added and the mixture was gently stirred for 2 h. The solvent was removed under vacuum, and then the NPs were resuspended in 20 mL of NaOH 0.05 M. To remove the excess of unbound polymer the solution was centrifuged at 25 000 rpm for 2 h twice.To obtain NPs from group B, 1% of the polymer monomers were modified with tetramethylrhodamine 5(6)-carboxamide cadaverine (TAMRA) (Anaspec) under stirring for 12 h in 5 mL of chloroform before adding the NPs.

Coating NPs with Carbohydrates and PEG. Group A NPs were obtained by incubating 1 mg of NPs with 3 mg of *N*-(3-dimethylaminopropyl)-*N*′-ethylcarbodiimide hydrochloride (EDC), 25 μmoles of 4-aminophenyl β-D-glucopyranoside, 4-aminophenyl β-D-galactopyranoside or α-methoxy-ω-amino poly(ethylene glycol) 750 Da (Rapp Polymere) in 250 μL of SSB buffer pH 9 (50 mM of boric acid and 50 mM of sodium borate). After 15 min of incubation 0.4 μmoles of TAMRA were added. After 2 h the ligand excess was removed by washing the NPs with phosphate buffered saline (PBS) pH 7.4 in a centrifugal filter with a 100 000 Da molecular weight cut off membrane (Millipore).

Group B NPs were obtained following the same protocol with the exception of the addition of TAMRA.

General Procedures for Nanoparticles Characterization. Dynamic light scattering and zeta-potential measurements were performed on a Brookhaven Zeta PALS instrument at 25 °C. Each sample was measured three times, combining 10 runs per measurement.

Viability Testing. Cell viability was analyzed using the Quick Cell Proliferation Testing Solution (GenScript). Different cell lines were used in order to achieve a more complete study: HeLa (human cervical cancer cells), A549 (lung carcinoma cells), Vero (monkey kidney epithelial cells), and Raw 264.7 (mouse leukemic monocyte/macrophage cell line) were maintained in RPMI (Gibco) supplemented with 10% heat inactivated fetal calf serum (PAA), penicillin (100 U mL^{-1}), streptomycin (100 μg mL^{-1}), and glutamine (2 mM)(Gibco). A total of 15000 cells (HeLa, A549, Vero) and 20000 cells from Raw 264.7 were seeded using a standard 96-well plate (Falcon). NPs at different concentrations (50 and 100 μg mL^{-1}) and cells were incubated for 48 h at 37 °C in a humidified atmosphere containing 5% CO_2. The reaction was performed following the manufacturer instructions and was followed by spectrophotometric measurements at 450 nm with a microplate reader (Multiskan EX, BioAnalysis Labsytems). Control wells including cells treated with Triton X100 or just with NPs in medium (in the absence of cells) (Abs(NPs)) were analyzed as NPs can show absorbance at that wavelength. All experiments were repeated in triplicate twice. Results are shown as percent of viability (%V) according to the following formula:

$$\%V = \frac{\text{Abs(NPs + cells)} - \text{Abs(NPs)}}{\text{Abs(cells)} - \text{Abs(medium)}} 100$$

Statistical analyses were performed using OriginPro 8 software. An ANOVA with a Bonferroni *posthoc* test was performed comparing the different groups to the control cells. In all cases, a *P* value less than 0.01 was considered statistically significant.

ROS Production. HMy2 lymphoblastoid B leukemia cells were used to investigate the intracellular ROS generation: 250000 cells were exposed to 0.1 mg mL^{-1} NPs for 5 and 15 min. 2(,7(-Dichlorofluorescein−diacetate (DCFH-DA) (Invitrogen) (5 μM) was added to detect and quantify intracellular production of H_2O_2. In the presence of ROS produced during oxidative stress, the compound is oxidized and emits bright green fluorescence. The fluorescence was recorded by exciting the solution with a 488 nm argon laser using a FACS Coulter (FC500 MPL).

Complement Activation. Complement activation experiments were performed by Western Blot analysis. Equal volumes (20 μL each) of NPs (0.2 mg mL^{-1}), human plasma from three healthy donors and veronal buffer were mixed together and incubated at 37 °C for 60 min. As positive control, 6 U of Cobra Venom Factor (CVF) (Quidel Corporation) was used and PBS as negative control. Proteins were resolved using SDS-PAGE. Before the samples were loaded on the gel, sample buffer containing 2% of sodium dodecyl sulfate (SDS) and 0.5% of β-mercapthoethanol was mixed with the NPs and heated for 5 min at 90 °C. The mixture was centrifuged at 13 400 rpm for 30 min, and 1 μL of the supernatant was loaded on a 10% Tris-glycine gel. The samples were allowed to run for 1 h at 125 V and then were transferred to a membrane (Immunoblot PVDF membrane, BioRad) for 90 min at 100 mA using a semidry transfer cell (Trans blot SD, BioRad). The membrane was extensively washed with TBS-T (20 mM Tris, 140 mM NaCl, and 0.1% Tween-20) prior to incubating it overnight at 4 °C with 5% of nonfat dry milk in TBS-T (blocking buffer), on a rocking platform. The membrane was then washed and incubated with the primary antibody solution, consisting in a mouse monoclonal antibody against human C3 (Abcam) diluted 1:1000 in blocking buffer for 90 min. After another washing step, it was incubated with polyclonal goat antimouse IgG antibodies conjugated with alkaline phosphatase (Dako), diluted 1:2000 in blocking buffer for 90 min. The membrane was finally incubated with a solution containing Nitroblue Tetrazolium (NBT) and 5-bromo-4-chloro-3-indolyl phosphate (BCIP). This substrate system produces an insoluble NBT diformazan end product that is blue to purple in color and can be observed visually.

NPs Uptake Assays. Vero cells (ATCC number CCL-81) were grown at 37 °C in a 5% CO_2 atmosphere in Dulbecco's modified Eagle's medium (DMEM) (Lonza) supplemented with 10% fetal bovine serum (FBS). Vero cells, grown on glass coverslips to 30% confluence, were serum starved for 30 min; different types of NPs (final concentration, 0.1 mg mL^{-1}) in DMEM were added for 20 min at 4 °C for binding. Cells were then cold washed with DMEM and transferred to 37 °C for different times, where the uptake took place. NPs that were not internalized were removed by acid washing with 0.1 M NaCl−0.1 M glycine, pH 3.0. Cells were fixed for 10 min at room temperature with 200 μL of 4% paraformaldehyde, washed twice with PBS and incubated for 10 min with TO-PRO (Invitrogen) for nuclei labeling. The coverslips were mounted on glass microscope slides. Confocal microscopy was carried out in a Leica TCS SPE confocal microscope using a 63X objective, and images were analyzed using ImageJ.

Drug Treatments and Confocal Microscopy. Stock solutions of inhibitors were prepared as follows: 10 mM dynasore (DYN) (Calbiochem) and 5 mM nystatin (NYS) were prepared in dimethyl sulfoxide (DMSO). Chlorpromazine (CHZ) (20 mM)

and chloroquine (CLQ) (100 nM) were prepared in water. Working concentrations were already set up ensuring that cell death, determined by the trypan blue exclusion method, did not exceed 10% after incubation of cell cultures with the different inhibitors. Cells were pretreated for 30 min with inhibitors at the desired final concentrations (80 μM DYN, 50 μM NYS, 14 μM CHZ, and 20 μM CLQ) in DMEM at 37 °C. NPs at a final concentration of 0.1 mg mL^{-1} were cold incubated with the cells (20 min) and cold washes with DMEM were done prior to incubation with the inhibitors at the same concentrations. Control experiments were performed using 50 μg mL^{-1} Alexa Fluor 594-labeled human Transferrin (TF) (Molecular Probes). Cells were then transferred to 37 °C for the uptake experiment (20 min) and, as before, NPs or TF that were not internalized were removed by acid washing with 0.1 M NaCl−0.1 M glycine, pH 3.0. Cells were fixed for 10 min at room temperature with 200 μL of 4% paraformaldehyde, washed twice with PBS and incubated for 10 min with TO-PRO (Invitrogen) for nuclei labeling. The coverslips were mounted on glass microscope slides. Confocal microscopy was carried out in a Leica TCS SPE confocal microscope using a 63× objective.

NPs internalized in cells were quantified by measuring fluorescence intensities, performing the image analyses with Leica Application Suite advanced fluorescence software. For a given experiment, the settings on the microscope were kept constant for all the samples, including exposures, pinhole size, and PMT gain. The samples were scanned at different locations.

Cholera Toxin (CT) and NPs Colocalization. Cholera toxin subunit B (1 μg mL^{-1}) from *Vibrio cholerae* labeled with Alexa Fluor A488 (Molecular Probes) was incubated for 20 min at 4 °C with 0.1 mg mL^{-1} of NPs in DMEM, after Vero cells were serum starved for 30 min. Cells were cold washed with DMEM and transferred to 37 °C for 15 min and 4 h. Cells were fixed for 10 min at room temperature with 200 μL of 4% paraformaldehyde, washed twice with PBS, and incubated for 10 min with DAPI for nuclei labeling. The coverslips were mounted on glass microscope slides. Confocal microscopy was carried out in an Olympus Fluoview FV10i confocal microscope equipped with a 60× objective. Specificity of labeling and absence of signal crossover were determined by examination of single labeled control samples. Colocalized points were analyzed using ImageJ.

Lysotracker Colocalization Assays. Vero cells seeded on 35 mm Petri dish (Ibidi) were incubated with glucose NPs for 12 h as previously described. Afterward they were loaded with 75 nM LysoTracker green (Invitrogen) for 30 min and imaged live. Live imaging of cells was performed using an Olympus Fluoview FV10i confocal microscope equipped with a 60× objective. The specificity of labeling and the absence of signal crossover were determined by examination of single-labeled control samples.

Acknowledgment. This work was supported by ERC-Starting Grant-NANOPUZZLE, CONSOLIDER CSD2006-12, CONSOLIDER CSD2006-00007, AGL2009-0209, and CTQ2008-03739/PPQ projects from ERC and Spanish Ministry of Science and Innovation. J. M. de la Fuente thanks ARAID for financial support. B. Sáez thanks ISCIII for financial support (Sara Borrell Program CD09/00174). The authors thank I. Echaniz and S. Rivera for technical support. The authors thank Dra. M. Royo (I+CS/IIS) and J. Godino (I+CS/IIS) for technical assistance with the confocal microscope and flow cytometry analysis. The authors also thank C. Cuestas-Ayllon (LMA-INA) for technical assistance with SEM micrographs. We also thank F. Luvi and A. Bird for fruitful discussions

Supporting Information Available: Additional details of experiments and results (NP characterization, cytotoxicity, time-dependent NPs uptake, cell morphology, cytoskeleton staining, and NPs uptake) are included. This material is available free of charge *via* the Internet at http://pubs.acs.org.

REFERENCES AND NOTES

1. Sanvicens, N.; Marco, M. P. Multifunctional Nanoparticles: Properties and Prospects for Their Use in Human Medicine. *Trends Biotechnol.* **2008**, *26*, 425–433.
2. Pankhurst, Q. A.; Thanh, N. K. T.; Jones, S. K.; Dobson, J. Progress in Applications of Magnetic Nanoparticles in Biomedicine. *J. Phys. D: Appl. Phys.* **2009**, *42*, 224001.
3. Jain, K. K. Nanotechnology in Clinical Laboratory Diagnostics. *Clin. Chim. Acta* **2005**, *358*, 37–54.
4. Mahmoudi, M.; Sant, S.; Wang, B.; Laurent, S.; Sen, T. Superparamagnetic Iron Oxide Nanoparticles (SPIONs): Development, Surface Modification and Applications in Chemotherapy. *Adv. Drug Delivery Rev.* **2011**, *63*, 24–46.
5. Berry, C. C. Progress in Functionalization of Magnetic Nanoparticles for Applications in Biomedicine. *J. Phys. D: Appl. Phys.* **2009**, *42*, 224003.
6. Sperling, R. A.; Parak, W. J. Surface Modification, Functionalization and Bioconjugation of Colloidal Inorganic Nanoparticles. *Phil. Trans. R. Soc. A* **2010**, *368*, 1333–83.
7. Qiao, R.; Yang, C.; Gao, M. Superparamagnetic Iron Oxide Nanoparticles: From Preparations to *in Vivo* MRI Applications. *J. Mater. Chem.* **2009**, *19*, 6274–6293.
8. Veiseh, O.; Gunn, J. W.; Zhang, M. Design and Fabrication of Magnetic Nanoparticles for Targeted Drug Delivery and Imaging. *Adv. Drug Delivery Rev.* **2010**, *62*, 284–304.
9. Storm, G.; Belliot, S. O.; Daemen, T.; Lasic, D. D. Surface Modification of Nanoparticles to Oppose Uptake by the Mononuclear Phagocyte System. *Adv. Drug Delivery Rev.* **1995**, *17*, 31–48.
10. Moros, M.; Pelaz, B.; López-Larrubia, P.; García-Martin, M. L.; Grazú, V.; de la Fuente, J. M. Engineering Biofunctional Magnetic Nanoparticles for Biotechnological Applications. *Nanoscale* **2010**, *2*, 1746–1755.
11. Wang, M.; Thanou, M. Targeting Nanoparticles to Cancer. *Pharmacol. Res.* **2010**, *62*, 90–99.
12. Hakomori, S. Glycosylation Defining Cancer Malignancy: New Wine in an Old Bottle. *Proc. Natl. Acad. Sci. U.S.A.* **2002**, *99*, 10231–10233.
13. Varki, A. Biological Roles of Oligosaccharides: All of the Theories Are Correct. *Glycobiology* **1993**, *3*, 97–130.
14. de la Fuente, J. M.; Alcántara, D.; Penadés, S. Cell Response to Magnetic Glyconanoparticles: Does the Carbohydrate Matter? *IEEE Trans. Nanobiosci.* **2007**, *6*, 275–281.
15. El-Boubbou, K.; Zhu, D. C.; Vasileiou, C.; Borhan, B.; Prosperi, D.; Li, W.; Huang, X. Magnetic Glyco-Nanoparticles: A Tool to Detect, Differentiate, and Unlock the Glyco-Codes of Cancer *via* Magnetic Resonance Imaging. *J. Am. Chem. Soc.* **2010**, *132*, 4490–4499.
16. Sur, I.; Cam, D.; Kahraman, M.; Baysal, A.; Culha, M. Interaction of Multi-functional Silver Nanoparticles with Living Cells. *Nanotechnology* **2010**, *21*, 175104.
17. Bergen, J. M.; von Recum, H. A.; Goodman, T. T.; Massey, A. P.; Pun, S. H. Gold Nanoparticles as a Versatile Platform for Optimizing Physicochemical Parameters for Targeted Drug Delivery. *Macromol. Biosci.* **2006**, *6*, 506–516.
18. Yoo, M. K.; Kim, I. Y.; Kim, E. M.; Jeong, H.-J.; Lee, C.-M.; Jeong, Y. Y.; Akaike, T.; Cho, C. S. Superparamagnetic Iron Oxide Nanoparticles Coated with Galactose-Carrying Polymer for Hepatocyte Targeting. *J. Biomed. Biotechnol.* **2007**, *2007*, ID 94740.
19. Marradi, M.; Alcántara, D.; de la Fuente, J. M.; García-Martín, M. L.; Cerdán, S.; Penadés, S. Paramagnetic Gd-Based Gold Glyconanoparticles as Probes for MRI: Tuning Relaxivities with Sugars. *Chem. Commun.* **2009**, *26*, 3922–3924.
20. Rabinovitch, M. Professional and Non-professional Phagocytes: An Introduction. *Trends Cell Biol.* **1995**, *5*, 85–87.
21. Sahay, G.; Alakhova, D. Y.; Kabanov, A. V. Endocytosis of Nanomedicines. *J. Controlled Release* **2010**, *145*, 182–195.
22. Hillaireau, H.; Couvreur, P. Nanocarriers' Entry into the Cell: Relevance to Drug Delivery. *Cell. Mol. Life Sci.* **2009**, *66*, 2873–2896.
23. França, A.; Aggarwal, P.; Barsov, E. V.; Kozlov, S. V.; Dobrovolskaia, M. A.González-Fernández, A. Macrophage Scavenger Receptor A Mediates the Uptake of Gold Colloids by Macrophages *in Vitro*. *Nanomedicine (London)* **2011**, *6*, 1175.
24. Osaki, F.; Kanamori, T.; Sando, S.; Sera, T.; Aoyama, Y. A Quantum Dot Conjugated Sugar Ball and Its Cellular Uptake. On the Size Effects of Endocytosis in the Subviral Region. *J. Am. Chem. Soc.* **2004**, *126*, 6520–6521.

25. Ahmed, M.; Deng, Z.; Liu, S.; Lafrenie, R.; Kumar, A.; Narain, R. Cationic Glyconanoparticles: Their Complexation with DNA, Cellular Uptake, and Transfection Efficiencies. *Bioconjugate Chem.* **2009**, *20*, 2169–2176.
26. El-Boubbou, K.; Huang, X. Glyco-nanomaterials: Translating Insights from the "Sugar-Code" to Biomedical Applications. *Curr. Med. Chem.* **2011**, *18*, 2060–2078.
27. Sun, S.; Zeng, H.; Robinson, D. B.; Raoux, S.; Rice, P. M.; Wang, S. X.; Li, G. Monodisperse MFe_2O_4 (M = Fe, Co, Mn) Nanoparticles. *J. Am. Chem. Soc.* **2004**, *126*, 273–279.
28. Pellegrino, T.; Manna, L.; Kudera, S.; Liedl, T.; Koktysh, D.; Rogach, A. L.; Keller, S.; Rädler, J.; Natile, G.; Parak, W. J. Hydrophobic Nanocrystals Coated with an Amphiphilic Polymer Shell: A General Route to Water Soluble Nanocrystals. *Nano Lett.* **2004**, *4*, 703–707.
29. Lemarchand, C.; Gref, R.; Couvreur, P. Polysaccharide-Decorated Nanoparticles. *Eur. J. Pharm. Biopharm.* **2004**, *58*, 327–341.
30. Sperling, R. A.; Liedl, T.; Duhr, S.; Kudera, S.; Zanella, M.; Lin, C. A. J.; Chang, W. H.; Braun, D.; Parak, W. J. Size Determination of (Bio)conjugated Water-Soluble Colloidal Nanoparticles: A Comparison of Different Techniques. *J. Phys. Chem. C* **2007**, *111*, 11552–11559.
31. Lewinski, N.; Colvin, V.; Drezek, R. Cytotoxicity of Nanoparticles. *Small* **2008**, *4*, 26–49.
32. Díaz, B.; Sánchez-Espinel, C.; Arruebo, M.; Faro, J.; de Miguel, E.; Magadán, S.; Yagüe, C.; Fernández-Pacheco, R.; Ibarra, M. R.; Santamaría, J.; *et al*. Assessing Methods for Blood Cell Cytotoxic Responses to Inorganic Nanoparticles and Nanoparticle Aggregates. *Small* **2008**, *4*, 2025–2034.
33. Shen, H.; Lin, Y.; Choksi, S.; Tran, J.; Jin, T.; Chang, L.; Karin, M.; Zhang, J.; Liu, Z.-G. Essential Roles of Receptor-Interacting Protein and TRAF2 in Oxidative Stress-Induced Cell Death. *Mol. Cell. Biol.* **2004**, *24*, 5914–5922.
34. Soenen, S. J. H.; Himmelreich, U.; Nuytten, N.; De Cuyper, M. Cytotoxic Effects of Iron Oxide Nanoparticles and Implications for Safety in Cell Labelling. *Biomaterials* **2011**, *32*, 195–205.
35. Gao, L.; Zhuang, J.; Nie, L.; Zhang, J.; Zhang, Y.; Gu, N.; Wang, T.; Feng, J.; Yang, D.; Perrett, S.; *et al*. Intrinsic Peroxidase-Like Activity of Ferromagnetic Nanoparticles. *Nat. Nanotechnol.* **2007**, *2*, 577–583.
36. Mahmoudi, M.; Azadmanesh, K.; Shokrgozar, M. A.; Journeay, W. S.; Laurent, S. Effect of Nanoparticles on the Cell Life Cycle. *Chem. Rev.* **2011**, *111*, 3407–3432.
37. Mahmoudi, M.; Simchi, A.; Imani, M. Cytotoxicity of Uncoated and Polyvinyl Alcohol Coated Superparamagnetic Iron Oxide Nanoparticles. *J. Phys. Chem. C* **2009**, *113*, 9573–9580.
38. AshaRani, P. V.; Mun, G. L. K.; Hande, M. P.; Valiyaveettil, S. Cytotoxicity and Genotoxicity of Silver Nanoparticles in the Human Lung Cancer Cell Line, A549. *ACS Nano* **2009**, *3*, 279–290.
39. Sim, R. B.; Tsiftsoglou, S. A. Proteases of the Complement System. *Biochem. Soc. Trans.* **2004**, *32*, 21–27.
40. Dobrovolskaia, M. A.; Patri, A. K.; Zheng, J.; Clogston, J. D.; Ayub, N.; Aggarwal, P.; Neun, B. W.; Hall, J. B.; McNeil, S. E. Interaction of Colloidal Gold Nanoparticles with Human Blood: Effects on Particle Size and Analysis of Plasma Protein Binding Profiles. *Nanomedicine* **2009**, *5*, 106–117.
41. Bertholon, I.; Vauthier, C.; Labarre, D. Complement Activation by Core–Shell Poly (isobutylcyanoacrylate)–Polysaccharide Nanoparticles: Influences of Surface Morphology, Length, and Type of Polysaccharide. *Pharm. Res.* **2006**, *23*, 1313–1323.
42. Salvador-Morales, C.; Flahaut, E.; Sim, E.; Sloan, J.; Green, M. L. H.; Sim, R. B. Complement Activation and Protein Adsorption by Carbon Nanotubes. *Mol. Immunol.* **2006**, *43*, 193–201.
43. Silverstein, S. C.; Steinman, R. M.; Cohn, Z. A. Endocytosis. *Annu. Rev. Biochem.* **1977**, *46*, 669–722.
44. Zhang, S.; Li, J.; Lykotrafitis, G.; Bao, G.; Suresh, S. Size-Dependent Endocytosis of Nanoparticles. *Adv. Mater.* **2009**, *21*, 419–424.
45. Mosqueira, V. C. F.; Legrand, P.; Gulik, A.; Bourdon, O.; Gref, R.; Labarre, D.; Barratt, G. Relationship Between Complement Activation, Cellular Uptake, and Surface Physicochemical Aspects of Novel PEG-Modified Nanocapsules. *Biomaterials* **2001**, *22*, 2967–79.
46. Verma, A.; Uzun, O.; Hu, Y.; Hu, Y.; Han, H.-S.; Watson, N.; Chen, S.; Irvine, D. J.; Stellacci, F. Surface-Structure-Regulated Cell-Membrane Penetration by Monolayer-Protected Nanoparticles. *Nat. Mater.* **2008**, *7*, 588–95.
47. Oh, E.; Delehanty, J. B.; Sapsford, K. E.; Susumu, K.; Goswami, R.; Blanco-Canosa, J. B.; Dawson, P. E.; Granek, J.; Shoff, M.; Zhang, Q.; *et al.* Cellular Uptake and Fate of PEGylated Gold Nanoparticles Is Dependent on Both Cell-Penetration Peptides and Particle Size. *ACS Nano* **2011**, *5*, 6434–6448.
48. Xia, T.; Kovochich, M.; Liong, M.; Zink, J. I.; Nel, A. E. Cationic Polystyrene Nanosphere Toxicity Depends on Cell-Specific Endocytic and Mitochondrial Injury Pathways. *ACS Nano* **2008**, *2*, 85–96.
49. Otsuka, H.; Nagasaki, Y.; Kataoka, K. PEGylated Nanoparticles for Biological and Pharmaceutical Applications. *Adv. Drug Delivery Rev.* **2003**, *55*, 403–419.
50. Alexis, F.; Pridgen, E.; Molnar, L. K.; Farokhzad, O. C. Factors Affecting the Clearance and Biodistribution of Polymeric Nanoparticles. *Mol. Pharm.* **2008**, *5*, 505–515.
51. Li, S. D.; Huang, L. High Density but Sheddable PEG Is a Key for Tumor Targeting. *J. Controlled Release* **2010**, *145*, 178–181.
52. Mayor, S.; Pagano, R. E. Pathways of Clathrin-Independent Endocytosis. *Nat. Rev. Mol. Cell Biol.* **2007**, *8*, 603–612.
53. Williams, Y.; Byrne, S.; Bashir, M.; Davies, A.; Whelan, A.; Gun'ko, Y.; Kelleher, D.; Volkov, Y. Comparison of Three Cell Fixation Methods for High Content Analysis Assays Utilizing Quantum Dots. *J. Microsc. (Oxford, U. K.)* **2008**, *232*, 91–98.
54. Doherty, G. J.; McMahon, H. T. Mechanisms of Endocytosis. *Annu. Rev. Biochem.* **2009**, *78*, 857–902.
55. Hayer, A.; Stoeber, M.; Ritz, D.; Engel, S.; Meyer, H. H.; Helenius, A. Caveolin-1 Is Ubiquitinated and Targeted to Intralumenal Vesicles in Endolysosomes for Degradation. *J. Cell. Biol.* **2010**, *191*, 615–629.
56. Damke, H. Dynamin and Receptor-Mediated Endocytosis. *FEBS Lett.* **1996**, *389*, 48–51.
57. Henley, J. R.; Krueger, E. W. A.; Oswald, B. J.; McNiven, M. A. Dynamin-Mediated Internalization of Caveolae. *J. Cell. Biol.* **1998**, *141*, 85–99.
58. Sever, S.; Damke, H.; Schmid, S. L. Dynamin:GTP Controls the Formation of Constricted Coated Pits, the Rate Limiting Step in Clathrin-Mediated Endocytosis. *J. Cell. Biol.* **2000**, *150*, 1137–1148.
59. Macia, E.; Ehrlich, M.; Massol, R.; Boucrot, E.; Brunner, C.; Kirchhausen, T. Dynasore, a Cell-Permeable Inhibitor of Dynamin. *Dev. Cell.* **2006**, *10*, 839–850.
60. Wang, L.-H.; Rothberg, K. G.; Anderson, R. G. W. Mis-assembly of Clathrin Lattices on Endosomes Reveals a Regulatory Switch for Coated Pit Formation. *J. Cell. Biol.* **1993**, *123*, 1107–1117.
61. Hernaez, B.; Alonso, C. Dynamin- and Clathrin-Dependent Endocytosis in African Swine Fever Virus Entry. *J. Virol.* **2010**, *84*, 2100–2109.
62. de Duve, C. Lysosomes Revisited. *Eur. J. Biochem.* **1983**, *137*, 391–397.
63. Anderson, H. A.; Chen, Y.; Norkin, L. C. Bound Simian Virus 40 Translocates to Caveolin-enriched Membrane Domains, and Its Entry Is Inhibited by Drugs that Selectively Disrupt Caveolae. *Mol. Biol. Cell* **1996**, *7*, 1825–1834.
64. Harding, C.; Heuser, J.; Stahl, P. Receptor-mediated Endocytosis of Transferrin and Recycling of the Transferrin Receptor in Rat Reticulocytes. *J. Cell. Biol.* **1983**, *97*, 329–339.
65. Janes, P. W.; Ley, S. C.; Magee, A. I. Aggregation of Lipid Rafts Accompanies Signaling *via* the T Cell Antigen Receptor. *J. Cell. Biol.* **1999**, *147*, 447–461.
66. Torgersen, M. L.; Skretting, G.; van Deurs, B.; Sandvig, K. Internalization of Cholera Toxin by Different Endocytic Mechanisms. *J. Cell. Sci.* **2001**, *114*, 3737–3747.
67. Chithrani, B. D.; Chan, W. C. W. Elucidating the Mechanism of Cellular Uptake and Removal of Protein-Coated Gold

Nanoparticles of Different Sizes and Shapes. *Nano Lett.* **2007**, *7*, 1542–1550.
68. Wang, Z.; Tiruppathi, C.; Minshall, R. D.; Malik, A. B. Size and Dynamics of Caveolae Studied Using Nanoparticles in Living Endothelial Cells. *ACS Nano* **2009**, *3*, 4110–4116.
69. Zhang, L. W.; Monteiro-Riviere, N. A. Mechanisms of Quantum Dot Nanoparticle Cellular Uptake. *Toxicol. Sci.* **2009**, *110*, 138–155.
70. Al-Hajaj, N. A; Moquin, A.; Neibert, K. D.; Soliman, G. M.; Winnik, F. M.; Maysinger, D. Short Ligands Affect Modes of QD Uptake and Elimination in Human Cells. *ACS Nano* **2011**, *5*, 4909–18.
71. Kovács, T.; Kárász, A.; Szöllosi, J.; Nagy, P. The Density of GM1-Enriched Lipid Rafts Correlates Inversely with the Efficiency of Transfection Mediated by Cationic Liposomes. *Cytometry, Part A* **2009**, *75A*, 650–7.
72. de Farias, P. M. A.; Santos, B. S.; Menezes, F. D.; Brasil, A. G., Jr.; Ferreira, R.; Motta, M. A.; Castro-Neto, A. G.; Vieira, A. A. S.; Silva, D. C. N.; Fontes, A.; *et al*. Highly Fluorescent Semiconductor Core−Shell CdTe−CdS Nanocrystals for Monitoring Living Yeast Cells Activity. *Appl. Phys. A: Mater. Sci. Process.* **2007**, *89*, 957–961.
73. Al-Hasani, H.; Hinck, C. S.; Cushman, S. W. Endocytosis of the Glucose Transporter GLUT4 Is Mediated by the GTPase Dynamin. *J. Biol. Chem.* **1998**, *273*, 17504–17510.
74. Lehmann, A. D.; Parak, W. J.; Zhang, F.; Ali, Z.; Röcker, C.; Nienhaus, G. U.; Gehr, P.; Rothen-Rutishauser, B. Fluorescent−Magnetic Hybrid Nanoparticles Induce a Dose-Dependent Increase in Proinflammatory Response in Lung Cells *in Vitro* Correlated with Intracellular Localization. *Small* **2010**, *6*, 753–762.
75. Sen, D.; Deerinck, T. J.; Ellisman, M. H.; Parker, I.; Cahalan, M. D. Quantum Dots for Tracking Dendritic Cells and Priming an Immune Response *in Vitro* and *in Vivo*. *PloS One* **2008**, *3*, e3290.
76. Jiang, X.; Röcker, C.; Hafner, M.; Brandholt, S.; Dörlich, R. M.; Nienhaus, G. U. Endo- and Exocytosis of Zwitterionic Quantum Dot Nanoparticles by Live HeLa Cells. *ACS Nano* **2010**, *4*, 6787–97.
77. Bareford, L. M.; Swaan, P. W. Endocytic Mechanisms for Targeted Drug Delivery. *Adv. Drug Delivery Rev.* **2007**, *59*, 748–758.
78. Pelkmans, L.; Kartenbeck, J.; Helenius, A. Caveolar Endocytosis of Simian Virus 40 Reveals a New Two-Step Vesicular-Transport Pathway to the ER. *Nat. Cell Biol.* **2001**, *3*, 473–483.
79. Dwek, R. A. Glycobiology: Toward Understanding the Function of Sugars. *Chem. Rev.* **1996**, *96*, 683–720.